ADVANCED ELECTRONIC MATERIALS
www.advelectronicmat.de

Defect Self-Compensation for High-Mobility Bilayer InGaZnO/In_2O_3 Thin-Film Transistor

Jiawei He, Guoli Li, Yawei Lv, Chunlan Wang, Chuansheng Liu, Jinchai Li, Denis Flandre, Huipeng Chen, Tailiang Guo, and Lei Liao**

Here, the bilayer InGaZnO/In_2O_3 thin-film transistors (TFTs) are deposited by radio-frequency magnetron sputtering at room temperature. A high field-effect mobility (μ_{FE}) of 64.4 $cm^2 V^{-1} s^{-1}$ and a small subthreshold swing (SS) of 204 mV per decade are achieved in the bilayer-stack TFTs fabricated upon SiO_2/Si substrate, with large improvement compared to the single-layer InGaZnO and In_2O_3 TFTs. Implementing HfO_2 and Si_3N_4 as high-*k* gate dielectrics, μ_{FE} and SS are correspondingly enhanced to be 67.5 and 79.1 $cm^2 V^{-1} s^{-1}$, and 85 and 92 mV per decade in the bilayer TFTs. Defect self-compensation effect is also revealed, i.e., $(In)^+ + (O)^- \rightarrow In - O$, while, respectively, considering the indium- and oxygen-related defects in InGaZnO and In_2O_3 and exploring the numerical simulations in SILVACO/Atlas (for electrical performance) and Quantum Espresso (for physical analysis). The In—O formation can result in a significant reduction in defect density (validated by the X-ray photoelectron spectra and low-frequency noise characterizations) and therefore improvement of μ_{FE} and SS in the bilayer-stack TFT. The important role of defect self-compensation mechanism while combining different individual channel layers in the oxide semiconducting TFTs is underlined and highly potential application in next-generation, fast-speed flexible displays is shown.

1. Introduction

Metal oxide semiconductors, e.g., ZnO,[1,2] In_2O_3,[3] InZnO (IZO),[4] ZnSnO,[5] InGaZnO (IGZO),[6] AlZnSnO,[7] and InZnSnO,[8,9] have been rapidly adopted as the active channel materials of thin-film transistors (TFTs), since the first amorphous IGZO (a-IGZO) TFT was fabricated by Hosono and coworkers and presented impressive electron mobility and current on/off ratio.[10,11] Taking advantage of their excellent optical transparency, high mechanical flexibility, and especially low-temperature process feasibility, the amorphous oxide semiconducting (AOS) TFTs have triggered large scientific interests and industrial benefits, and can be widely used in active-matrix liquid crystal display, bio- and optical sensing fields, etc.[12]

However, disordered structural network and high density of intrinsic defects in the AOS materials largely affect electrical performances (e.g., electron mobility and stability) of the TFTs and limit their industrial applications in next-generation electronic device platforms. To overcome these limitations, a notable strategy, i.e., stacked-layer channel combining different individual oxide semiconducting materials, has been proposed in recent years and successfully implemented to enhance the device performances.[13–19] Park and Lee reported a bilayer IZO/IGZO TFT with the field-effect mobility (μ_{FE}) of 47.7 $cm^2 V^{-1} s^{-1}$ and threshold voltage (V_{TH}) of 1.57 V, where the mobility enhancement (i.e., ≈2.3 times higher than that of a single-layer IGZO TFT) was induced by a high electron density of the IGZO layer with electrons injected from the IZO layer of the stacked structure.[13] Liu et al. presented

J. He, Dr. C. Liu, Prof. J. Li, Prof. L. Liao
School of Physics and Technology
Wuhan University
Wuhan 430072, China
E-mail: liaolei@whu.edu.cn

Dr. G. Li, Dr. Y. Lv, Prof. D. Flandre, Prof. L. Liao
Key Laboratory for Micro-/Nano-Optoelectronic Devices
of Ministry of Education
School of Physics and Electronics
Hunan University
Changsha 410082, China
E-mail: liguoli_lily@hnu.edu.cn

The ORCID identification number(s) for the author(s) of this article can be found under https://doi.org/10.1002/aelm.201900125.

DOI: 10.1002/aelm.201900125

Dr. C. Wang
School of Science
Xi'an Polytechnic University
Xi'an 710048, China

Prof. D. Flandre
Institute of Information and Communication Technologies
Electronics and Applied Mathematics
Université catholique de Louvain
1348, Louvain-la-Neuve, Belgium

Prof. H. Chen, Prof. T. Guo
Institute of Optoelectronic Display
Fuzhou University
Fuzhou 350002, China

a high-performance In_2O_3 (front channel)/IZO (back channel) TFT, showing an increased μ_{FE} of 37.9 $cm^2\ V^{-1}\ s^{-1}$ and thereafter a decreased subthreshold swing (SS) of 120 mV decade, where the thin (3–7 nm) In_2O_3 layer was regarded as the main accumulation and transportation layer due to its amorphous structure and high μ_{FE} (100 $cm^2\ V^{-1}\ s^{-1}$).[14] Abliz et al. demonstrated electrical performance enhancement in a bilayer IGZO:H/IGZO TFT, achieving μ_{FE} of 55.3 $cm^2\ V^{-1}\ s^{-1}$ and SS of 0.18 V decade by inserting an ultrathin (5 nm) hydrogenated IGZO layer to provide suitable carrier concentration and reduce the average trap density near the channel/insulator interface.[15] Kim et al. successfully fabricated the high-performance oxide TFTs composed of the IZO (or InSnO) and IGZO active layers, showing μ_{FE} of 51.3 $cm^2\ V^{-1}\ s^{-1}$ (104 $cm^2\ V^{-1}\ s^{-1}$), but the insight physics remained unexplored.[19] The superior performance parameters of the stacked-layer TFTs in refs[16–18] were attributed to the formation of 2D electron gas (2DEG) at the heterointerface between the respective metal oxide film, where the 2DEG-like system formed in the TFTs requires careful tuning of the quantized energy level in the semiconducting layers (e.g., In_2O_3/ZnO and In_2O_3/Al_2O_3) as well as the suitable device architectures to enable a band-like electron transport.[20]

Investigation pertaining to using the stacked-layer channel in TFTs is still in the nascent stage. Despite the carrier accumulation, 2DEG creation, and the exotic interface property discussed earlier, how intrinsic defects and their possible interactions affect device performances in the stacked-layer TFTs has not been considered yet. As it is well known, there is high density of intrinsic defects existing in the AOS materials, including the dangling bonds, atoms, impurities, etc.[21,22] The intrinsic defects can be mainly divided into three categories: 1) the point defects including the peroxide (O—O, acting as donor) and the metal–metal bond (or small metal cluster, M—M, acting as acceptor), 2) the stoichiometric defects including the oxygen vacancy (V_O, donor) and oxygen interstitial (O_i, acceptor), and 3) the impurities like the metal–hydrogen and oxygen–hydrogen bonds, depending on the AOS material.[23] While considering the bond dissociation energy between metal and oxygen atoms, e.g., In—O, Zn—O, and Ga—O,[24] it is crucial to understand formation of these intrinsic defects (dangling bond, atom, or cluster) and their possible interactions (i.e., defect self-compensation mechanism) in the stacked-layer TFT.[21,25]

The defect self-compensation may provide a more viable approach for the multilayer TFT application; however, it remains largely unexplored to date. In this work, we will deposit the amorphous IGZO and In_2O_3 films at room temperature (RT) and investigate the superior device performances in the bilayer-stack IGZO/In_2O_3 TFT by experiments and simulations, thereafter to reveal insights into the defect self-compensation effect in TFT technology and physics.

2. Results and Discussion

Figure 1a,b illustrates the schematics of the single-layer and bilayer back-gated TFTs, respectively, with device channel length (L) of 120 µm and width (W) of 150 µm in this research. Transfer characteristics (i.e., drain–source current versus gate voltage, I_{DS}–V_{GS}) of the single-layer (25 nm thick) IGZO and In_2O_3, and the bilayer (5/20 nm thick) IGZO/In_2O_3 TFTs measured at RT and V_{DS} = 1 V are shown in Figure 1c with field-effect mobility μ_{FE} extracted by

$$\mu_{FE} = \frac{g_m L}{W V_{DS} C_{ox}} \quad (1)$$

where g_m and C_{ox}, respectively, represent the transconductance and gate-dielectric capacitance per unit area.[24] In Figure 1c,

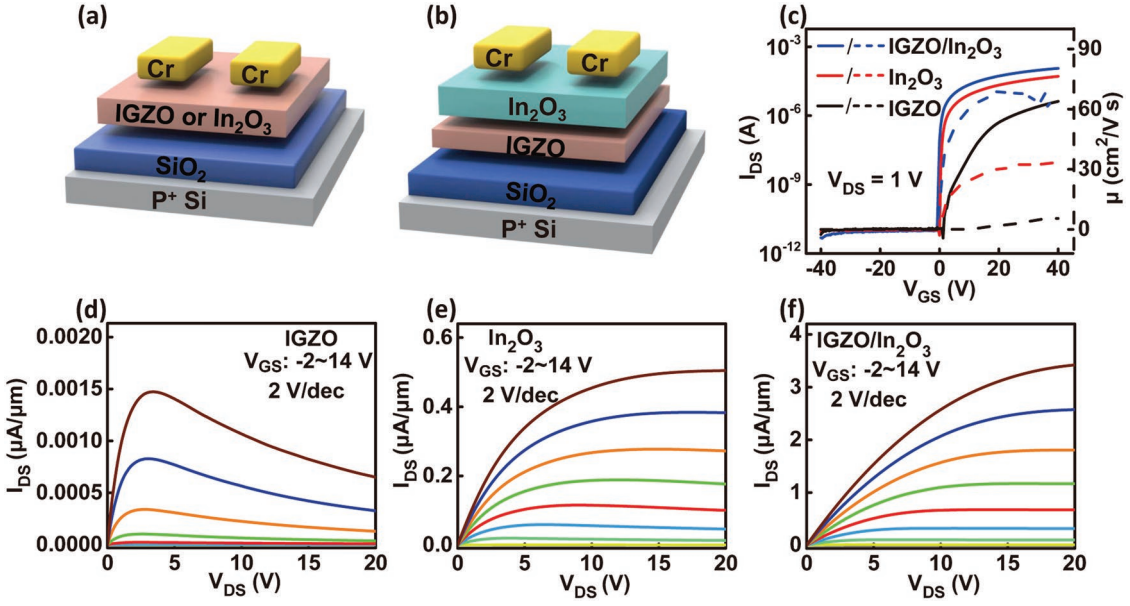

Figure 1. a,b) Schematics of the single-layer IGZO or In_2O_3 and bilayer IGZO/In_2O_3 TFTs. c) Transfer characteristics (solid line in the left) and field-effect mobility (dash line in the right) of the three TFTs at V_{DS} = 1 V, measured at room temperature. d–f) Output characteristics of the single-layer IGZO and In_2O_3, and the bilayer IGZO/In_2O_3 TFTs.

Table 1. Extracted electrical characteristics in the single-layer and bilayer AOS TFTs fabricated by room-temperature sputtering.

Structure	V_{TH} [V]	μ_{FE} [cm^2 V^{-1} s^{-1}]	SS [mV per decade]	I_{on}/I_{off}	N_t [cm^{-3} eV^{-1}]	ΔV_{TH} [V]
IGZO	5.0	5.3	647	6.3×10^5	1.2×10^{20}	15.1
In_2O_3	0.5	29.8	223	5.9×10^6	1.1×10^{18}	7.9
IGZO/In_2O_3	–0.3	64.4	204	2.5×10^7	2.4×10^{16}	1.8
30 nm HfO_2	–0.2	67.5	85	3.9×10^7	–	0.1
50 nm Si_3N_4	–0.3	79.1	92	3.3×10^7	–	2.0

the bilayer IGZO/In_2O_3 TFT obviously achieves the enhanced electrical performances, with a high μ_{FE} of 64.4 cm^2 V^{-1} s^{-1}, a high current on/off ratio (I_{on}/I_{off}) of 2.5×10^7, a low V_{TH} of –0.3 V, and a small SS of 204 mV decade, in comparison with μ_{FE} of 5.3 and 29.8 cm^2 V^{-1} s^{-1}, I_{on}/I_{off} of 6.3×10^5 and 5.9×10^6, V_{TH} of 5.0 and 0.5 V, and SS of 647 and 223 mV decade in the single-layer IGZO and In_2O_3 TFTs, respectively. Electrical performance parameters are extracted and listed in **Table 1**. It is worth noting that, generally, μ_{FE} is largely affected by the subgap defects, while SS is mainly determined by the deep-level traps existing in the AOS channel layer.[26] Output curves (i.e., drain–source current versus drain voltage, I_{DS}–V_{DS}) of the single-layer IGZO and In_2O_3, and the bilayer IGZO/In_2O_3 TFTs are correspondingly depicted in Figure 1d–f, with gate voltage V_{GS} ranging from –2 to 14 V. The output current plateau reached in the bilayer TFT with the highest value of 3.4 μA μm^{-1}, in a distinct contrast to the current collapse phenomena observed in the single-layer IGZO TFT (Figure 1d). In the experiments, while increasing the V_{DS} (positive value), the band of IGZO material close to the drain electrode bends down, which results in more acceptors in the IGZO film getting ionized by capturing electrons and thereafter leads to the decrease of the output current.[27–29] It demonstrates that the improved device performances in the bilayer IGZO/In_2O_3 TFTs are related to the decreased defect density compared with the current collapse of the single-layer IGZO TFT, from another aspect. It is also worth mentioning that the specific thickness combination (5/20 nm) of the bilayer IGZO/In_2O_3 reported in this work is the optimal case that we have achieved and verified by several sessions of the experiments. Although enhancement in the device electrical performances has also been observed in other thickness combination and the bilayer stack (e.g., In_2O_3/IGZO), they all show the poor performances when compared to those of the bilayer IGZO/In_2O_3 TFT.

To identify corresponding intrinsic defects in the two individual AOS materials, sputtering temperature effect on the device characteristics is investigated in the single-layer IGZO and In_2O_3 TFTs. **Figure 2**a,b shows the hysteresis plots (as well as the transfer curves) of the single-layer IGZO and In_2O_3 TFTs deposited at different temperatures, i.e., RT, 100, and 150 °C. While increasing the sputtering temperature, device performances (e.g., V_{TH}, SS, and threshold voltage difference (ΔV_{TH}) between the forward and backward curves in hysteresis plots) have been obviously enhanced in the single-layer IGZO TFT,[30] whereas a large negative shift in the transfer characteristics is observed and high conductivity is induced in the single-layer In_2O_3 TFT. Therefore, while increasing the sputtering temperature, the different trends shown in the electrical performances

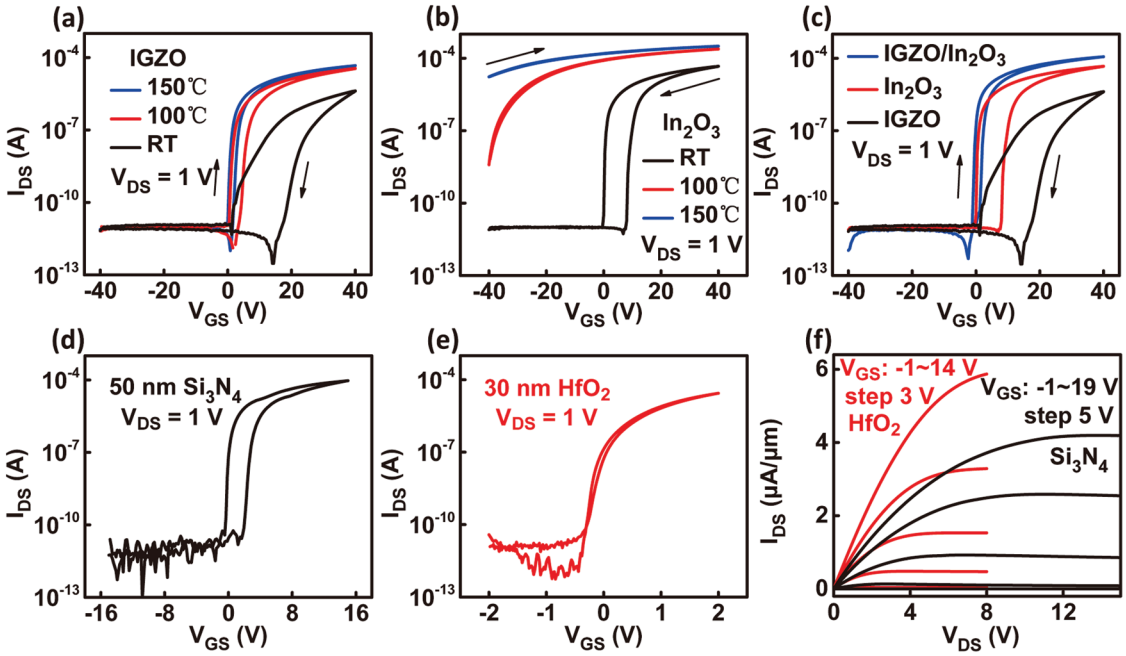

Figure 2. a,b) Hysteresis curves measured at V_{DS} = 1 V in the single-layer IGZO and In_2O_3 TFTs deposited at different temperatures of RT, 100, and 150 °C. c) Hysteresis curves measured at V_{DS} = 1 V in the single-layer IGZO and In_2O_3, and the bilayer IGZO/In_2O_3 TFTs deposited at RT. d,e) Transfer and f) output characteristics of the bilayer IGZO/In_2O_3 TFTs with high-k gate dielectrics (Si_3N_4 and HfO_2), measured at V_{DS} = 1 V.

of the two single-layer TFTs indicate different types of the dominant defects, i.e., the indium-related defects in In_2O_3 and the oxygen-related defects in IGZO.[31–33] More detailed discussion will be given next.

Combining the two individual materials, the hysteresis characteristics of the bilayer IGZO (5 nm thick)/In_2O_3 (20 nm thick) TFT deposited at RT are shown in Figure 2c. As listed in Table 1, ΔV_{TH} of the bilayer IGZO/In_2O_3 TFTs is reduced to 1.8 V using the 100 nm thick SiO_2 as the gate dielectric, which shows a large improvement compared to ΔV_{TH} of 15.1 and 7.9 V in the single-layer IGZO and In_2O_3 TFTs, respectively. As stated in ref. [34], the hysteresis degradation is commonly attributed to the hole/electron trapping in the interface of gate insulator and the creation of ionized oxygen vacancy in IGZO. The superior hysteresis performance in the bilayer-stack IGZO/In_2O_3 TFT indicates the reduced density of defects in the IGZO layer, i.e., defect self-compensation effect interacting between the IGZO and In_2O_3 materials and the IGZO/In_2O_3 interface. While using the 50 nm thick Si_3N_4 and 30 nm thick HfO_2 as the gate insulators,[35,36] the device transfer characteristics are, respectively, presented in Figure 2d,e, and the output curves are correspondingly depicted in Figure 2f. Thanks to the use of high-k dielectrics, further improvement in SS has been achieved in the bilayer IGZO/In_2O_3TFT with the demonstrated enhancement in μ_{FE}, as listed in Table 1. In the bilayer-stack TFT with the HfO_2 gate dielectric, SS has been decreased to 85 mV decade and ΔV_{TH} is optimized to be 0.1 V, with μ_{FE} of 67.5 $cm^2\ V^{-1}\ s^{-1}$. Meanwhile the device ON-state saturation current has been increased to 5.9 $\mu A\ \mu m^{-1}$ at V_{GS} = 14 V, with I_{on}/I_{off} reaching up to 3.9×10^7. In the Si_3N_4-insulating TFT, SS has been decreased to 92 mV decade with μ_{FE} of 79.1 $cm^2\ V^{-1}\ s^{-1}$.

In a-IGZO, one well-known mechanism is that oxygen vacancies (V_O) dominate in the intrinsic defect framework and dope the material by directly providing electrons to the conduction band, i.e., generating two free electrons and working as the donors.[23,30] As a result, the added oxygen interstitials (O_i) induced by the V_O and the ionized oxygen vacancies (V_O^+) act as acceptors and degrade device SS and hysteresis characteristics in the a-IGZO TFTs,[23,32] as depicted in Figure 2a. While increasing the sputtering temperature, these oxygen-related defect densities can be reduced.[26,30] In In_2O_3, the indium interstitials (In_i) act as the dominant defects, with the absolutely essential coexistence of the oxygen vacancies. However, V_O in In_2O_3 is hardly ionized, retaining two electrons near V_O.[33] The indium interstitial (atom, cluster, or metal with dangling bond[23]) generating a trap energy level close to the conduction band can supply free conduction electrons in In_2O_3, and In_i is consequently ionized to be positive $(In_i)^{n+}$ (n = 1, 2, 3).[37,38] To obtain the insight physics relevant to the single-layer IGZO and In_2O_3, and the bilayer IGZO/In_2O_3 TFTs, the 2D numerical simulations are first performed in SILVACO/Atlas to model the hysteresis characteristics that are mainly governed by the deep energy states in the slow measurements,[34,39] with the device geometry and structure described in the Experimental Section. Taking example from SILVACO about the IGZO hysteresis by controlling the trapping and detrapping process of the deep energy states, we use direct transient simulation by adjusting capture cross section (i.e., 1e–25 cm^2), and set the ramping time to be 100 ms, which is consistent with the experimental settings while conducting the measurements. Simulation results of the single-layer IGZO and In_2O_3, and the bilayer IGZO/In_2O_3 TFTs are presented in **Figure 3**a and are in well agreement with the experimental observations in Figure 2c. The superior hysteresis performance (e.g., smaller ΔV_{TH}) of the bilayer-stack TFT qualitatively validates the reduced defect density ($5 \times 10^{17}\ eV^{-1}\ cm^{-3}$) in the bilayer IGZO/$In_2O_3$ TFT, compared to the defect densities of $6 \times 10^{18}\ eV^{-1}\ cm^{-3}$ (oxygen-related defects) and $3 \times 10^{18}\ eV^{-1}\ cm^{-3}$ (indium-related defects) separately implemented into the single-layer IGZO and In_2O_3 TFTs. Based on the aforementioned defects in IGZO and In_2O_3 materials, the inset of Figure 3a depicts the band diagram and corresponding defect description of IGZO and In_2O_3 after contact.[40] When an In_2O_3

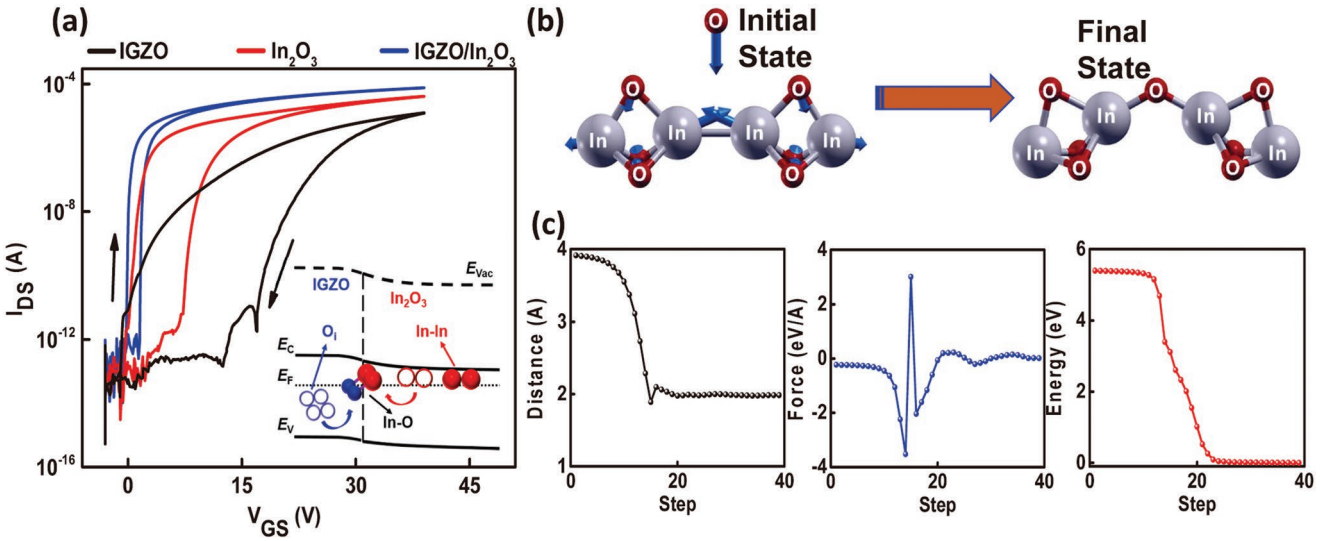

Figure 3. a) Hysteresis modeling in the single-layer IGZO and In_2O_3, and the bilayer IGZO/In_2O_3 TFTs, in SILVACO/Atlas. The inset depicts the band diagram and defect description of IGZO and In_2O_3 after contact. b) Initial and final states of the intervention, in Quantum Espresso. c) Distance, force, and energy variation along the BFGS searching step, based on the DFT calculation.

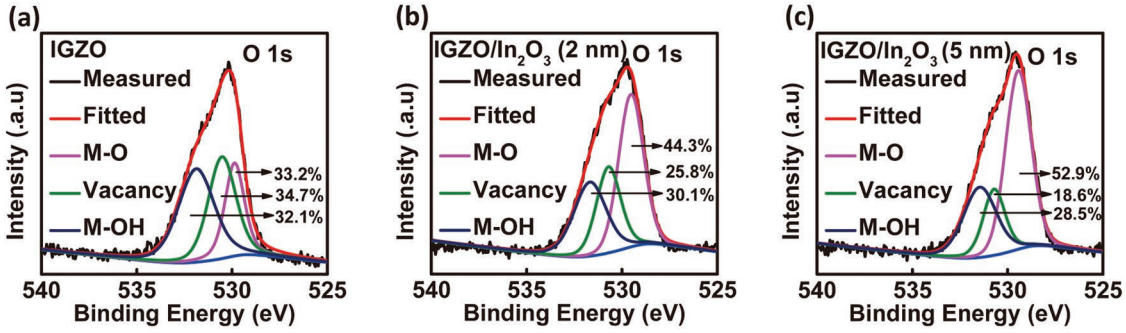

Figure 4. The XPS O 1s spectra analyzed in three types of the oxide TFTs, constructed by a) the single-layer (5 nm thick) IGZO, b) the bilayer (5/2 nm thick) IGZO/In_2O_3, and c) the bilayer (5/5 nm thick) IGZO/In_2O_3.

layer contacts with an ultrathin (5 nm thick) IGZO film, the oxygen atom acting as anion capturing electrons (i.e., oxygen interstitial O_i, acceptor[23]) in the IGZO layer is proposed to interact with the indium atom with dangling bond (i.e., metal cluster or In atom[23,24]) in the In_2O_3 layer in this research. The formation of the In—O separations can be in the range of 2.0–2.23 Å and close to the ideal bond length (In—O) with the high bond dissociation energy of 346 kJ mol^{-1},[37] therefore leading to the reduced defect densities and the enhanced performances in the bilayer IGZO/In_2O_3 TFTs. This defect self-compensation effect could be symbolically expressed by $(In)^+ + (O)^- \rightarrow In - O$.

Next, simulations by using first-principles density functional theory (DFT) in Quantum Espresso, with Perdew–Burke–Ernzerhof exchange-correlation functional and projector augmented-wave pseudopotential adopted, are done to analyze and demonstrate the bonding formation between the In and O atoms.[23,41] Figure 3b shows that the O atom is located 4 nm away from the two bonded In atoms (i.e., metal cluster) as the initial state, where the In_2O_3 system is fully relaxed until the total energy variations and forces are less than 1.4×10^{-3} eV and 2.6×10^{-2} eV $Å^{-1}$, respectively.[42] While using the BFGS quasi-Newton algorithm to search the minimum energy state of a system,[43] the O atom rapidly moves toward the bonded In atoms, reaching to a final distance of 2 Å after a brief fluctuation (Figure 3c, left). The fluctuation of the O atom position near the balance point causes large forces that can further avoid its escape (Figure 3c, middle). The whole process is energy favorable, since no barrier is seen in the energy variation (Figure 3c, right). In the final state, the In—In bond is replaced by two In—O bonds, verifying the defect self-compensation effect in the bilayer-stacked IGZO/In_2O_3 from the side of solid-state physics. Additionally, it is interesting to discuss here that the In $3d_{5/2}$ and O 1s chemical binding states illustrated in ref. [17] for the bulk (In_2O_3) and interface regions of the amorphous Al_2O_3/In_2O_3 heterostructure demonstrate the In—O bond dissociation and formation from chemical observations in the AOS material systems, where the remarkably reduced percentage of the In^{3+} states and correspondingly increased percentage of the In^{0-2+} states reveal the O extraction from metal atom upon the Al_2O_3 deposition process.

In order to further analyze the defect self-compensation effect, the X-ray photoelectron spectra (XPS) is obtained. The relative O 1s spectra of the (5 nm thick) IGZO, the (5/2 nm thick) IGZO/In_2O_3, and the (5/5 nm thick) IGZO/In_2O_3 films are analyzed, as shown in **Figure 4**. Gaussian fitting with the subtraction of a Shirley-type background is used to deconvolute the O 1s spectra into three different peaks (O_L, O_M, and O_H), centered at 529.9 ± 0.1, 530.7 ± 0.1, and 531.9 ± 0.1 eV, respectively.[44] The low binding energy peak (O_L) at 529.9 eV is associated with the O^{2-} ion of metal oxide, such as In—O bonds. The high binding energy peak (O_H) located at 531.9 eV is usually attributed to the OH^- species on the surface of thin film termed the specific chemisorbed oxygen, such as $-CO_3$ and H_2O. The peak at the middle binding energy of 530.7 eV (O_M) is correlated to O^{2-} ion of the oxygen-deficient species.[45] When the In_2O_3 layer thickness increased from 0 to 5 nm, the relative ratio of the O_M peak decreases and the percentage of O_L peak increases, which indicates that the defect density at the interface between the IGZO and In_2O_3 layers is reduced whereas the related M—O bonds increase. The peak area percentages of the three TFTs with different In_2O_3 layer thicknesses are extracted and listed in **Table 2**. Based on the XPS information, we further believe that the defects in the bilayer IGZO/In_2O_3 have been greatly reduced by the defect self-compensation effect. Also, we note that the IGZO and In_2O_3 films both have good surface roughness under atomic force microscopy, indicating that the surface roughness may have an active impact on device performance somehow, but not a big role in this research.

Finally, low-frequency noise (LFN) characterizations have been performed in these three types of amorphous TFTs fabricated upon the standard SiO_2/Si substrate, to clarify the trap densities in experiments. Usually, the Hooge's empirical relation can be used to describe the LFN[46]

$$S_{ID} = \frac{AI_D^{\alpha}}{f^{\beta}} \tag{2}$$

Table 2. XPS peak area percentages of the IGZO/In_2O_3 TFTs with different In_2O_3 film thicknesses.

$T_{In_2O_3}$	M—O	Vacancy	M—OH
0 nm	33.2%	34.7%	33.2%
2 nm	44.3%	25.8%	30.1%
5 nm	52.9%	18.6%	28.5%

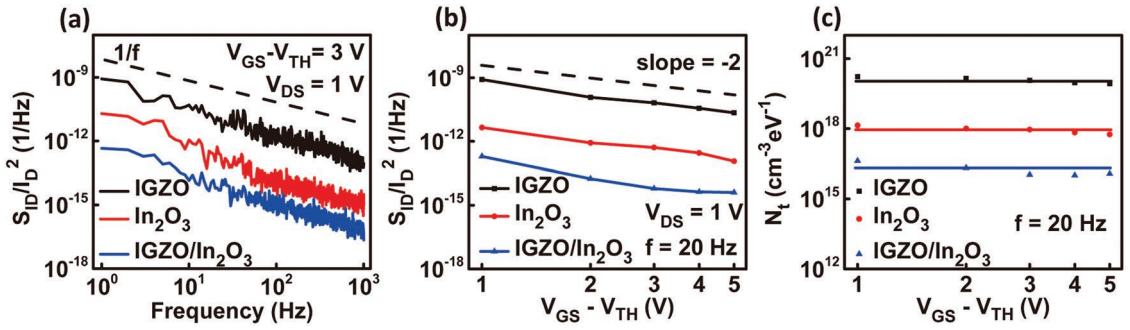

Figure 5. a) Normalized low-frequency noise spectra density (S_{ID}/I_D^2) in the single-layer IGZO and In_2O_3, and the bilayer IGZO/In_2O_3 TFTs, measured at $V_{GS} - V_{TH} = 3$ V and $V_{DS} = 1$ V. b) Log–log plots of the S_{ID}/I_D^2 versus $V_{GS} - V_{TH}$ at frequency = 20 Hz and $V_{DS} = 1$ V. c) Average interfacial trap density (N_t) as a function of the voltage $V_{GS} - V_{TH}$.

where S_{ID} is the current noise spectral density, f is the frequency, and A is a technology coefficient. The values of exponents α and β are dependent on the device and its operation mode, and are ideally close to 2 and 1, respectively. The normalized drain-current noise spectral density (S_{ID}/I_D^2) at RT fits well to the $1/f^{\beta}$ noise theory (f ranges from 1 to 1000 Hz), with the representative curves shown in **Figure 5**a at $V_{GS} - V_{TH} = 3$ V and $V_{DS} = 1$ V. The normalized S_D/I_D^2 in the bilayer IGZO/In_2O_3 TFT is obviously decreased compared to the two single-layer TFTs, which indicates the decreased average trap density in the bilayer stack.[26] A slope factor of –2 observed in the normalized S_{ID}/I_D^2 at $f = 20$ Hz and $V_{DS} = 1$ V (Figure 5b) validates the dominance of the carrier number fluctuation theory in the LFN,[26] which is caused by the electron trapping and detrapping at the SiO_2/IGZO interface. The average interfacial trap density (N_t) within the gate oxide can be extracted by

$$N_t = \frac{S_{ID} C_{ox}^2 WLf (V_{GS} - V_{TH})^2 \gamma}{q^2 kTI_D^2} \quad (3)$$

where γ is the attenuation coefficient of the electron wave function within the SiO_2 dielectric and has a value of 10^8 cm^{-1} for the Si/SiO_2 system.[27] The calculated N_t values in the three TFTs at $f = 20$ Hz are shown in Figure 5c with a uniform distribution, indicating its independence with respect to energy.[47] The calculated N_t values of 1.2×10^{20}, 1.1×10^{18}, and 2.4×10^{16} cm^{-3} eV^{-1}, respectively, for the single-layer IGZO and In_2O_3, and bilayer IGZO/In_2O_3 TFTs are in quantitative agreement with the aforementioned defect self-compensation and qualitatively validate the improvement in the device electrical performances, e.g., SS μ_{FE}, and ΔV_{TH}.

3. Conclusion

In summary, the bilayer (5/20 nm thick) IGZO/In_2O_3 AOS TFTs, which were fabricated by radio-frequency (RF) magnetron sputtering at RT, achieved enhanced electrical performances with μ_{FE} of 64.4 cm^2 V^{-1} s^{-1}, SS of 204 mV decade, I_{on}/I_{off} of 2.5×10^7, and ΔV_{TH} of 1.8 V, and further improvement in SS (85 mV decade), ΔV_{TH} (0.1 V), and μ_{FE} (79.1 cm^2 V^{-1} s^{-1}) was obtained when using the high-k gate dielectrics (HfO_2 and Si_3N_4). Taking account of the respective dominant defects in IGZO and In_2O_3 and regarding the bond formation, the defect self-compensation effect ($(In)^+ + (O)^- \rightarrow In - O$) was concluded in this work. The mechanism is consistent with the high bond dissociation energy of In—O validated by the DFT calculation and the XPS characterization, and results in the reduced defect density with the decreased hysteresis effect and LFN (in experiment and SILVACO simulation). The high-mobility IGZO/In_2O_3 TFTs deposited at RT in this research open up the possibility of developing high-resolution and fast-speed industrial TFT displays by using the stacked active-layer channel and shed light on the defect self-compensation in the AOS material systems at the low-temperature processing.

4. Experimental Section

First, a 30 nm thick HfO_2 layer was grown onto a heavily p-type doped silicon substrate by atomic layer deposition at temperature of 95 °C, using a KE-MICRO TALD-200A system. Then, the 5 nm thick IGZO film was separately deposited on the 30 nm thick HfO_2/p^+-Si substrates, 100 nm thick thermal SiO_2/p^+-Si substrates, and 50 nm thick Si_3N_4/p^+-Si substrates by RF magnetron sputtering at RT. During the sputtering deposition, the RF power was 50 W, the Ar flow rate was 9.0 sccm, and the gas pressure was 0.7 Pa. Subsequently, the 20 nm thick In_2O_3 layer was deposited on the ultrathin IGZO layer by RF magnetron sputtering at RT. During the sputtering process, the RF power was 50 W, the Ar flow rate was 9.0 sccm, and the gas pressure was 0.8 Pa. The 15/50 nm thick Cr/Au layers were finally deposited to form the source and drain electrodes by thermal evaporation. In the experiments, both the channel layers and the source/drain electrodes were patterned by shadow mask. Besides, the single-layer TFTs (with the 25 nm thick IGZO or In_2O_3) were also fabricated for comparison.

The electrical measurements were performed at Lake Shore TTPX Probe Station and Keysight B2912A semiconductor parameter analyzer in air. The thickness of the IGZO and In_2O_3 films was measured by J. A. Woollam M-2000 ellipsometer. The low-frequency noise characterizations were carried out by NC300L LFN analyzer under ambient conditions.

Acknowledgements

J.H. and G.L. contributed equally to this work. This work was supported by National Key Research and Development Program of China (nos. 2016YFB0401103 and 2016YFF0203600), the National Natural Science Foundation of China (nos. 11575132, 11574083, and 11664038), and the Natural Science Foundation of Hunan Province (nos. 2017RS3021 and 2017JJ3033).

Conflict of Interest

The authors declare no conflict of interest.

Keywords

amorphous oxide semiconductor, bilayer stack, defect self-compensation, high mobility, thin-film transistor

Received: January 30, 2019
Revised: March 17, 2019
Published online:

[1] Y. Y. Lin, C. C. Hsu, M. H. Tseng, J. J. Shyue, F. Y. Tsai, *ACS Appl. Mater. Interfaces* **2015**, *7*, 22610.
[2] H. Bong, W. H. Lee, D. Yun, B. J. Kim, J. H. Cho, K. Cho, *Appl. Phys. Lett.* **2010**, *96*, 192115.
[3] Y. Meng, G. X. Liu, A. Liu, H. J. Song, *RSC Adv.* **2015**, *5*, 37807.
[4] J. Z. Sheng, H. J. Lee, S. Oh, J. S. Park, *ACS Appl. Mater. Interfaces* **2016**, *8*, 33821.
[5] L. C. Liu, J. S. Chen, J. S. Jeng, *Appl. Phys. Lett.* **2014**, *105*, 023509.
[6] M. Mativenga, S. J. An, J. Jang, *IEEE Electron Device Lett.* **2013**, *34*, 1533.
[7] H. J. Jeon, W. J. Maeng, J. S. Park, *Ceram. Int.* **2014**, *40*, 8769.
[8] C. Avis, H. R. Hwang, J. Jang, *ACS Appl. Mater. Interfaces* **2014**, *6*, 10941.
[9] C. S. Liu, P. T. Liu, W. H. Huang, S. M. Sze, *IEEE Electron Device Lett.* **2014**, *35*, 1103.
[10] T. Kamiya, K. Nomura, H. Hosono, *Nature* **2004**, *432*, 488.
[11] H. Yabuta, T. Kamiya, H. Hosono, *Appl. Phys. Lett.* **2006**, *89*, 112123.
[12] E. Fortunato, P. Barquinha, R. Martins, *Adv. Mater.* **2012**, *24*, 2945.
[13] J. C. Park, H. Lee, *IEEE Electron Device Lett.* **2012**, *33*, 818.
[14] G. X. Liu, A. Liu, F. K. Shan, *Appl. Phys. Lett.* **2014**, *105*, 113509.
[15] A. Abliz, J. L. Wang, L. Xu, D. Wan, L. Liao, *Appl. Phys. Lett.* **2016**, *108*, 213501.
[16] J. Krausmann, S. Sanctis, J. Engstler, M. Luysberg, M. Bruns, J. J. Schneider, *ACS Appl. Mater. Interfaces* **2018**, *10*, 20661.
[17] S. Y. Lee, J. Kim, A. Park, J. Park, H. Seo, *ACS Nano* **2017**, *11*, 6040.
[18] H. Faber, S. Das, Y. H. Lin, N. Pliatsikas, K. Zhao, T. Kehagias, G. Dimitrakopulos, A. Amassian, P. A. Patsalas, T. D. Anthopoulosl, *Sci. Adv.* **2017**, *3*, e1602640.
[19] S. I. Kim, C. J. Kim, J. C. Park, I. Song, S. W. Kim, H. Yin, E. Lee, J. C. Lee, Y. Park, presented at *IEEE Int. Electron Devices Meeting*, San Francisco, CA, USA, December **2008**.
[20] J. G. Labram, Y. H. Lin, T. D. Anthopouls, *Small* **2015**, *11*, 5472.
[21] J. E. Stehr, K. M. Johansen, T. S. Bjørheim, L. Vines, B. G. Svensson, W. M. Chen, I. A. Buyanova, *Phys. Rev. Appl.* **2014**, *2*, 021001.
[22] H. Z. Zhang, H. T. Cao, A. H. Chen, L. Y. Liang, Z. M. Liu, Q. Wan, *Solid-State Electron.* **2010**, *54*, 479.
[23] A. de Jamblinne de Meux, G. Pourtois, J. Genoe, P. Heremans, *Phys. Rev. Appl.* **2018**, *9*, 054039.
[24] N. Mitoma, S. Aikawa, X. Gao, T. Kizu, M. Shimizu, M. F. Lin, T. Nabatame, K. Tsukagoshi, *Appl. Phys. Lett.* **2014**, *104*, 102103.
[25] G. Miceli, A. Pasquarello, *Phys. Rev. B* **2016**, *93*, 165207.
[26] A. Abliz, Q. Gao, D. Wan, X. Liu, L. Xu, C. Liu, C. Jiang, X. Li, H. Chen, T. Guo, J. Li, L. Liao, *ACS Appl. Mater. Interfaces* **2017**, *9*, 10798.
[27] N. Noda, R. Tsurumaki, K. Horio, presented at *IEEE 11th Int. Conf. on Nitride Semiconductors*, Beijing, China, August **2015**.
[28] K. Horio, K. Yonemoto, H. Takayanagi, H. Nakano, *J. Appl. Phys.* **2005**, *98*, 124502.
[29] S. M. Sze, K. K. Ng, *Physics of Semiconductor Devices*, Wiley, Hoboken, NJ, USA **2007**.
[30] J. K. Yao, N. S. Xu, S. Z. Deng, *IEEE Trans. Electron Devices* **2011**, *58*, 1121.
[31] J. T. Jang, J. Park, B. D. Ahn, D. M. Kim, S Choi, H. Kim, D. H. Kim, *ACS Appl. Mater. Interfaces* **2015**, *7*, 15570.
[32] G. Li, A. Abliz, L. Xu, N. André, X. Q. Liu, Y. Zeng, D. Flandre, L. Liao, *Appl. Phys. Lett.* **2018**, *112*, 253504.
[33] T. Tomita, K. Yamashita, Y. Hayafuji, H. Adachi, *Appl. Phys. Lett.* **2005**, *87*, 051911.
[34] Y. J. Chen, Y. H. Tai, C. Y. Chang, *IEEE Trans. Electron Devices* **2016**, *63*, C4.
[35] Y. H. Lin, J. C. Chou, *J. Nanomater.* **2015**, *1*, 782786.
[36] R. Yao, Z. Zheng, M. Xiong, X. Zhang, X. Li, H. Ning, Z. Fang, W. Xie, X. Lu, J. Peng, *Appl. Phys. Lett.* **2018**, *112*, 103503.
[37] A. Walsh, C. R. A. Catlow, A. A. Sokol, A. M. Woodley, *Chem. Mater.* **2009**, *21*, 4962.
[38] J. Liu, T. Liu, F. Liu, H. Li, *RSC Adv.* **2014**, *4*, 36983.
[39] *Atlas User's Manual: Device Simulation Software*, Silvaco Inc., Santa Clara, CA, USA **2016**.
[40] W. Korner, D. F. Urban, C. Elsasser, *Phys. Status Solidi A* **2015**, *212*, 1476.
[41] P. Giannozzi, O. Andreussi, T. Brumme, O. Bunau, M. Buongiorno Nardelli, M. Calandra, R. Car, C. Cavazzoni, D. Ceresoli, M. Cococcioni, N. Colonna, I. Carnimeo, A. Dal Corso, S. de Gironcoli, P. Delugas, R. A. DiStasio, A. Ferretti, A. Floris, G. Fratesi, G. Fugallo, R. Gebauer, U. Gerstmann, F. Giustino, T. Gorni, J. Jia, M. Kawamura, H. Y. Ko, A. Kokalj, E. Küçükbenli, M. Lazzeri, M. Marsili, N. Marzari, F. Mauri, N. L. Nguyen, H. V. Nguyen, A. Otero-de-la-Roza, L. Paulatto, S. Poncé, D. Rocca, R. Sabatini, B. Santra, M. Schlipf, A. P. Seitsonen, A. Smogunov, I. Timrov, T. Thonhauser, P. Umari, N. Vast, X. Wu, S. Baroni, *J. Phys.: Condens. Matter* **2017**, *29*, 465901.
[42] H. Omura, H. Kumomi, K. Nomura, T. Kamiya, M. Hirano, H. Hosono, *J. Appl. Phys.* **2009**, 105.
[43] Y. Lv, A. Liu, Q. Huang, S. Chang, W. Qin, S. Ye, H. Wang, J. He, *IEEE Electron Device Lett.* **2018**, *39*, 1092.
[44] A. Abliz, C. W. Huang, J. L. Wang, L. Liao, *ACS Appl. Mater. Interfaces* **2016**, *8*, 7862.
[45] T. S. Kang, T. Y. Kim, G. M. Lee, H. C. Sohn, J. P. Hong, *J. Mater. Chem. C* **2014**, *2*, 1390.
[46] F. N. Hooge. *IEEE Trans. Electron Devices* **1994**, *41*, 1926.
[47] K. K. Hung, P. K. Ko, C. M. Hu, *IEEE Trans. Electron Devices* **1990**, *37*, 645.

